

Neutron Diffraction and Gravimetric Study of the Iron Nitriding Reaction under Ammonia Decomposition Conditions

Thomas J. Wood^{†*}, Joshua W. Makepeace^{††} and William I. F. David^{††*}

[†] ISIS Facility, Rutherford Appleton Laboratory, Harwell Oxford, Didcot, OX11 0QX, UK

^{††} Inorganic Chemistry Laboratory, University of Oxford, Oxford, OX1 3QR, UK

*Corresponding authors: thomas.wood@stfc.ac.uk, bill.david@stfc.ac.uk

ABSTRACT

Ammonia decomposition over iron catalysts is known to be affected by whether the iron exists in elemental form or as a nitride. In-situ neutron diffraction studies with simultaneous gravimetric analysis were performed on the nitriding and denitriding reactions of iron under ammonia decomposition conditions. The gravimetric analysis agrees well with the Rietveld analysis of the neutron diffraction data, both of which confirm that the form of the iron catalyst is strongly dependent on ammonia decomposition conditions. Use of ammonia with natural isotopic abundance as the nitriding agent means that the incoherent neutron scattering of any hydrogen within the gases present is able to be correlated to how much ammonia had decomposed. This novel analysis reveals that the nitriding of the iron occurred at exactly the same temperature as ammonia decomposition started. The iron nitriding and denitriding reactions are shown to be related to steps that take place during ammonia decomposition and the optimum conditions for ammonia decomposition over iron catalysts are discussed.

INTRODUCTION

Ammonia, NH_3 , is currently synthesised via the Haber-Bosch process on the 140-megatonne scale per year principally because of its use in the production of fertilizers.¹ Ammonia is also receiving a revived interest as a chemical energy store,^{2,3,4} due to favourable properties such as: its specific energy (5.2–6.2 kWh/kg depending on whether water is produced as gas or liquid), straightforward storage (liquid at 10 bar and room temperature) and the fact that accessing its stored energy (whether by combustion⁵ or fuel cell^{6,7,8}) only entails the release of environmentally benign nitrogen and water. While the Haber-Bosch process for ammonia synthesis is a mature, century-old technology, the decomposition of ammonia (which is highly desirable for using ammonia in both combustion engines⁹ and fuel cells) is less advanced and has been studied mostly with the motivation of furthering understanding NH_3 synthesis. The most active transition metal catalysts for ammonia decomposition reflect those for ammonia synthesis; that is, ruthenium¹⁰ (used in the Kellogg advanced ammonia process for ammonia synthesis) and iron (used in the Haber-Bosch reaction). Recently, however, light metal amides and imides have been found to be active catalysts

for ammonia decomposition,^{11,12} but even in these cases there is some evidence that the presence of transition metals such as iron or manganese is advantageous.^{13,14}

In the case of transition metals, the rate-limiting step of ammonia decomposition is normally nitrogen desorption ($2\text{N}_{(\text{ads})} \rightarrow \text{N}_{2(\text{g})}$).^{15,16} This is not the case for all transition metals—e.g. tungsten shows a rate-limiting step of N–H scission¹⁷—but does describe iron under normal ammonia decomposition conditions. The importance of whether iron exists in its elemental form or an iron nitride is recognized to be a critical factor in the reaction rate of ammonia decomposition with the reaction proceeding more rapidly on iron surfaces rather than nitride surfaces.^{18,19} Previous in-situ X-ray diffraction studies of iron catalysts under flowing ammonia have shown that increased ammonia decomposition is associated with conditions where the composition of the iron catalyst tends towards elemental iron rather than iron nitrides.²⁰

In this study, iron powder was heated under ammonia to ammonia decomposition temperatures (>400 °C) while, simultaneously, neutron diffraction and gravimetric data were collected. The sample mass data were able to be correlated to the neutron diffraction patterns. The use of neutron diffraction also allowed the parallel reactions of ammonia decomposition and iron nitriding/denitriding to be studied under non-flowing conditions (where the approximate gas composition can be determined from the strong incoherent neutron scattering of hydrogen) in order to determine the conditions under which the catalyst is iron or some form of iron nitride.

EXPERIMENTAL

In-situ neutron diffraction measurements were performed at the POLARIS diffractometer, ISIS Pulsed Neutron and Muon Source, UK using the Intelligent Gravimetric Analyser for Neutrons (IGAⁿ, Hiden Isochema). The experiment entailed the weighing out of around 785 mg of iron powder (98%, ~325 mesh, Alfa Aesar) into a quartz bucket under inert atmosphere (to prevent any oxidation). The bucket was then hung from a fine tungsten wire connected to a balance. A stainless steel tail surrounded the sample and the entire setup was lowered into the neutron beam. Furnace elements were located above and below the quartz bucket and a thermocouple was also positioned above. The pressure was controlled by an inlet and outlet valve such that gas did not flow through the system, but any local changes in pressure (e.g. release of gas by sample) were mitigated; this was achieved by the inlet valve opening if the gas pressure was below the pressure setpoint and the outlet valve opening if the gas pressure was above the pressure setpoint. A schematic of the setup is shown in Figure 1.

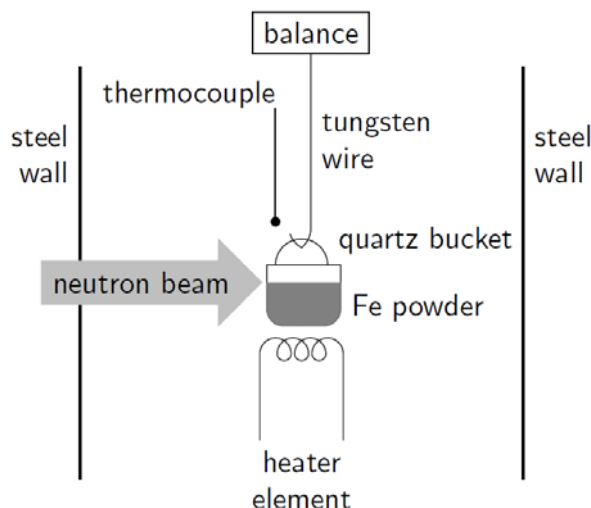


Figure 1: Schematic of experimental setup—not shown are the heater element above the quartz bucket (through which the tungsten wire goes) or the gas inlet and outlets.

In order to gain as much data as possible about the ammonia decomposition and iron nitriding/denitriding reactions, the experimental conditions were varied over time as follows: (i) an initial 30 minute scan was taken under an argon atmosphere at room temperature (to give a sample diffraction baseline) before the sample container region was evacuated of gas; (ii) ammonia (NH_3 , 99.98% SIP Analytical) was introduced at 1 bar and the sample was then heated to 450 °C (from time = 3.20 h to 6.6 h, with a short hiatus due to a pressure trip); (iii) sample kept at 450 °C and constant pressure (to time = 7.4 h); (iv) in an attempt to induce further nitriding of the sample, the ammonia pressure was increased to 1.2 bar, before three evacuation/ammonia refreshment (to 1.2 bar) cycles (to time = 10.0 h); (v) an evacuation/ammonia refreshment to 2 bar was then undertaken to maximise nitriding of the sample along with an increase in temperature to 480 °C (at time = 10.8 h); (vi) after sample denitriding, a series of evacuation/ammonia refreshment cycles were undertaken at different ammonia pressures (0.5, 0.6, 0.7, 0.8, 1 bar) at 480 °C in order to determine the effect of ammonia partial pressure on the denitriding reaction (to time = 18.2 h); (vii) to further determine the influence of temperature on the nitriding/denitriding reactions, the temperature was dropped to 420 °C and five ammonia evacuation/refreshment cycles (to 1 bar) were performed; (viii) finally, the sample was cooled (from time = 23.4 h) under ammonia and subsequently argon (from time=24.9 h). The temperature, pressure and gas compositions are shown in Figure 2.

Neutron diffraction data were analysed by Rietveld analysis using TOPAS v5 (Bruker AXS). The banks of detectors used for fitting the data were the backscattering bank (up to 2.62 Å) and the bank at 90° (up to 4.1 Å). Steel peaks were fitted by Pawley analysis using two different $\text{Fm}\bar{3}\text{m}$ phases corresponding to the reactor walls at neutron beam entry and exit points. Similarly, small peaks

pertaining to the thermocouple were fitted to an $Im\bar{3}m$ NiCr alloy phase. A previously collected silica scattering pattern was used as a scalable background to fit the scattering from the quartz bucket in conjunction with a Chebyshev polynomial function. Multiple datasets were refined using a batch process from a seed dataset, which had all phases present. The region between 2.01 Å and 2.17 Å was excluded from the 90° bank fitting because it comprised the largest steel (111) peaks overlapping with the largest (110) iron peak; its exclusion led to more stable fitting.

RESULTS & DISCUSSION

Identification of phases present

The diffraction data from the backscattering bank along with the mass, temperature and pressure traces are shown in Figure 2. Initially visible within the diffraction contour plot are double peaks due to the steel walls (corresponding to the neutron beam entry and exit—these peaks are at d-spacings of around 1.1 Å (311), 1.3 Å (220), 1.8 Å (200) and 2.1 Å (111)) as well as peaks corresponding to iron in the $Im\bar{3}m$ space group, comprising the (110) peak at 2.03 Å, the (200) peak at 1.43 Å and the (211) peak at 1.17 Å. After heating under ammonia (NH_3) to 450 °C, Fe_4N is formed (with a corresponding decrease in intensity in the iron peaks) in space group $Pm\bar{3}m$ with peaks for the following reflections: (311) at 1.15 Å, (220) at 1.34 Å, (221) at 1.55 Å, (210) at 1.70 Å, (200) at 1.90 Å and (111) at 2.20 Å (higher d-spacing reflections were visible in the 90° bank).

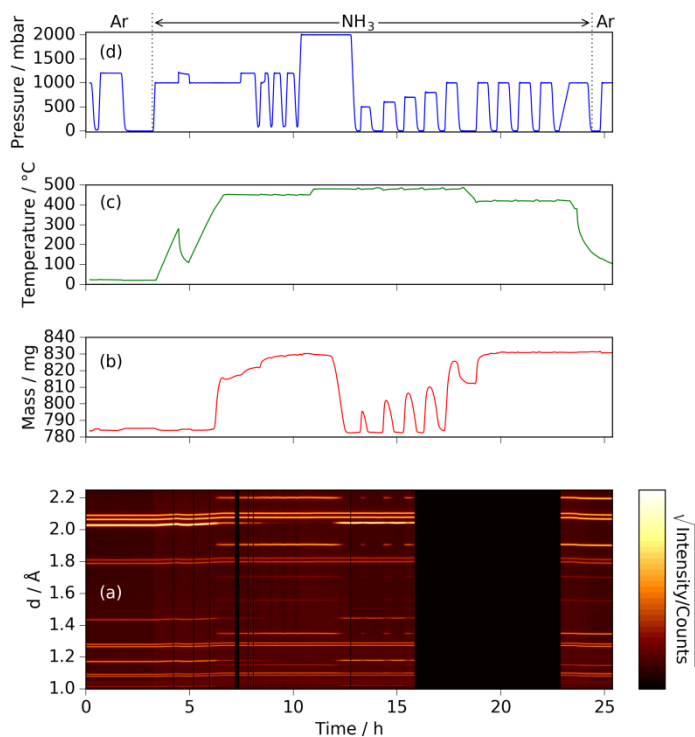


Figure 2: (a) Neutron powder diffraction data (black region between 16 and 23 h refers to time where neutron beam was unavailable); (b) mass of sample; (c) temperature of sample; (d) pressure within the IGAⁿ chamber (gas composition is shown at the top). The temperature dip between 4–5 h was due to a furnace trip error.

It can be seen that the appearance of the Fe₄N peaks corresponds to a significant mass gain in the sample, which is expected from the nitriding reaction. Rietveld analysis on all the diffraction datasets led to a fraction (by mass) of the Fe₄N present in the sample seen in Figure 3. This fraction determined by Rietveld analysis corresponded very well to the overall mass gain throughout the reaction, which indicates that no significant amounts of any amorphous phases were present (i.e. all phases were observed in the diffraction data).

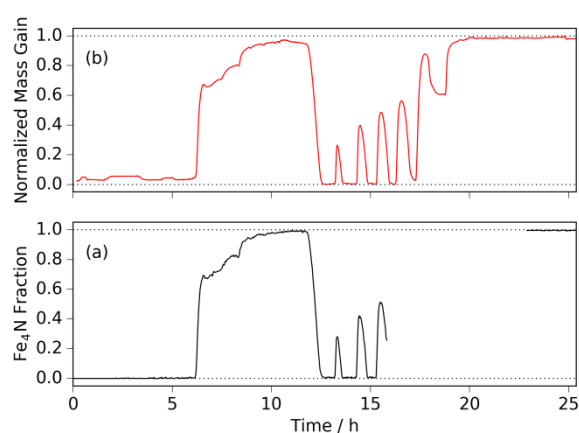


Figure 3: (a) Fe₄N fraction of the sample by mass as determined by Rietveld analysis (balance made up by Fe); (b) normalized mass gain of the sample, where 1 represents the expected mass from full conversion to Fe₄N.

It can also be seen that while the initial mass gain (and Fe₄N fraction rise) is sharp, it quickly plateaus and only rises again on the introduction of more NH₃ (pressure increase to 1.2 bar at 7.5 h). A second sharp (but smaller) increase in mass is seen when the gas is evacuated and more NH₃ is introduced (8.4 h), but there is a plateau shortly afterwards. Even after an increase in gas pressure to 2 bar (at 10.3 h) there is little increase in mass, but there is a slight discrepancy between the mass gain, which rises then dips again on the temperature being increased to 480 °C (at 10.9 h), whereas the Fe₄N fraction keeps approaching 1.0 (i.e. all Fe₄N). This discrepancy is explained by the formation of another nitride, Fe₃N, which can be seen in the diffraction data when it is summed over the relevant period (10.3–11.0 h). After this summation, a very small peak corresponding to the (211) reflection of Fe₃N in space group P6₃22 can be seen, Figure 4. The small fraction of this nitride explains the discrepancy between the mass gain and the Fe₄N fraction (seen in Figure 3).

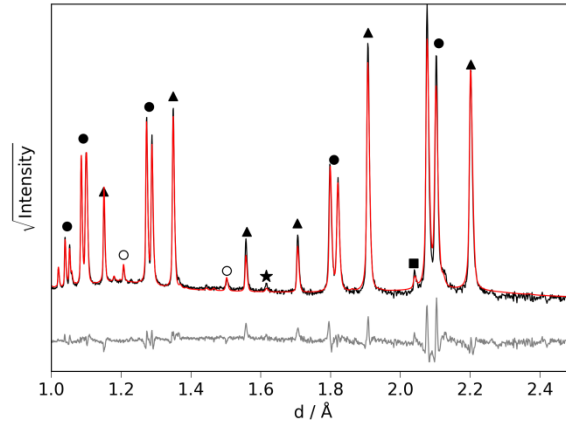


Figure 4: Sum of the neutron diffraction data for the backscattering bank between 10.3 h and 11.0 h (black); fit shown in red and difference in grey. The stainless steel doublets are denoted as filled circles (●), the thermocouple phase as open circles (○), Fe₄N peaks as filled triangles (▲), the Fe (110) peak as a filled square (■) and the Fe₃N (211) peak as a filled star (★).

Ammonia decomposition and its relationship to the iron nitriding/denitriding reactions

It can be seen (Figures 2 & 3) that the mass and Fe₄N fraction decrease rapidly between 11.8 and 12.5 h, i.e. the sample denitrides. This denitriding, along with the aforementioned plateau in the mass gain and Fe₄N fraction increase, can be attributed to the decomposition of the ammonia in the system to nitrogen and hydrogen ($2\text{NH}_3 \rightarrow \text{N}_2 + 3\text{H}_2$); H₂ enables denitriding of Fe₄N via the reaction $2\text{Fe}_4\text{N} + 3\text{H}_2 \rightarrow 2\text{NH}_3 + 4\text{Fe}$. This is consistent with previous in-situ X-ray diffraction studies of iron catalysts under flowing ammonia.²⁰

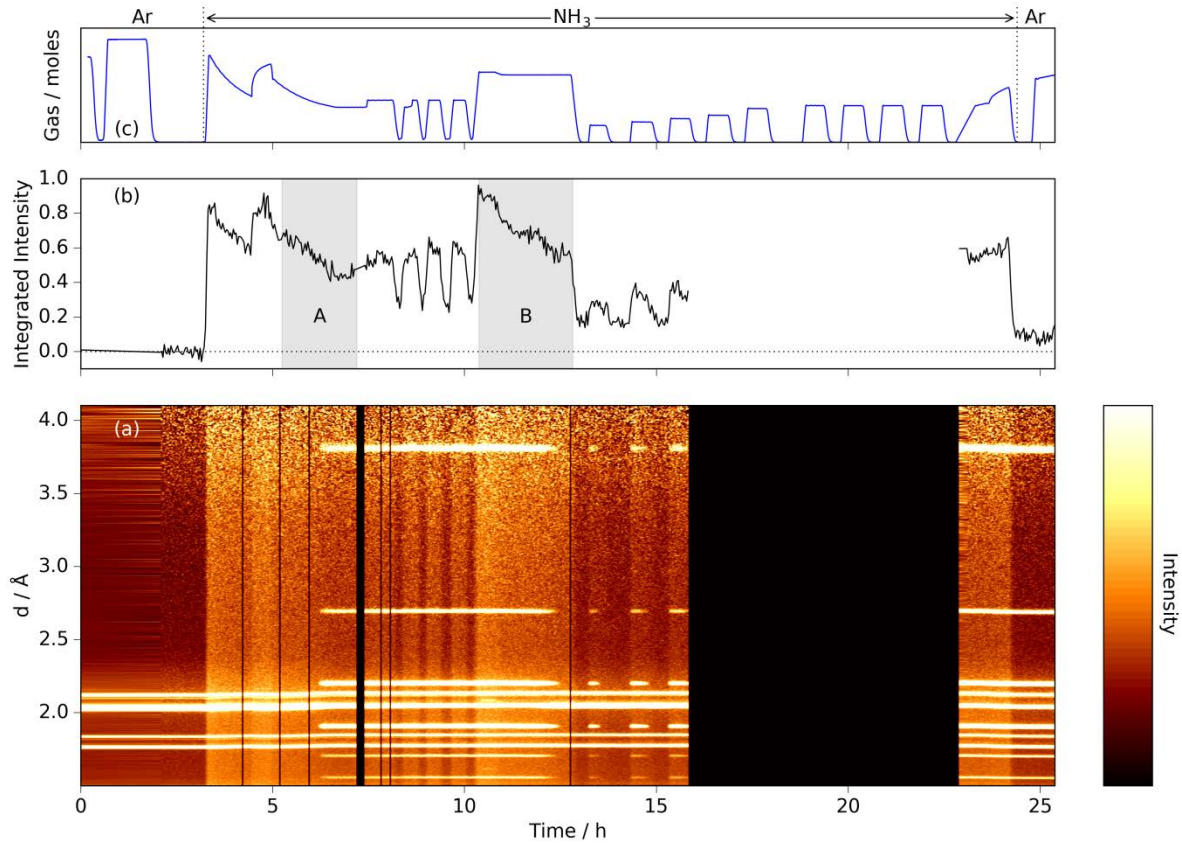
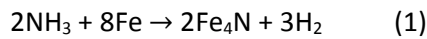


Figure 5: (a) Neutron diffraction data from the 90° scattering bank (z-scale limited so that background is emphasised); (b) the integrated background between the following regions: 1.95–1.98 Å, 2.3–2.65 Å, 2.75–3.25 Å and 3.5–3.75 Å, adjusted so that the region between 2.0 and 3.2 h corresponds to zero scattering; (c) the pressure divided by temperature (i.e. number of gas moles) and gas composition throughout.

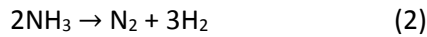
This decomposition can be correlated to the background of the diffraction data, since hydrogen nuclei have a large incoherent neutron scattering cross section. Integrating the background for the 90° bank between regions where there are no Bragg peaks leads to a trace that correlates with the pressure (and the temperature), Figure 5. Initially, when the sample is fully iron and under argon or vacuum (up to 3.2 h), the background consists of the incoherent scattering of (i) the sample and (ii) the steel walls as well as the scattering (coherent and incoherent) from the silica bucket (this is adjusted for in Figure 5(b)). At the end of the experiment (after 24.4 h), there is a small increase in the background relative to the starting level, which can be attributed to incoherent scattering from the nitrogen in the sample (which is close to fully Fe₄N)—this can also be thought of as a concentrating of the nitrogen from the gas in the IGAⁿ chamber (most of which is outside of the neutron beam) to the sample (all of which is illuminated by the neutron beam, see Figure 1). It is therefore possible to adjust the integrated background to take account of the amount of nitrogen in the sample (as determined from the mass gain and the Rietveld analysis). After 3.2 h, there is a large increase in the background, which is attributed to the introduction of NH₃ and the vast majority of

this increase is due to the hydrogen within the ammonia rather than the nitrogen as indicated by the relative magnitudes of their incoherent scattering cross-sections (80.26 barn and 0.5 barn respectively). The background scattering after that initial rise, however, decreases as temperature increases (and vice versa at 4.5 h, when the temperature decreases). These differences are due to the volume of the gas being kept constant, and so, for a given pressure, increasing the temperature will cause an exit of some gas from the system (which approximates to the ideal gas equation, $n = pV/RT$). Indeed, the whole integrated background trace may be adjusted to give a scattering (in arbitrary units) per mole of gas within the neutron beam by dividing by a factor of p/T (it should be noted that this relationship is only valid for similar pressures, otherwise the adsorption of gas on the sample/silica bucket/steel walls becomes significant). Once this is done (along with a small linear adjustment for the temperature attributed to changes in diffuse scattering), then the relative scattering can be directly correlated with the number of hydrogen atoms in the atmosphere surrounding the sample.

Once the relevant adjustments have been made, the only possible sources of a change in the scattering per mole of gas are the reaction of ammonia with iron to give iron nitride:



or the decomposition of ammonia into nitrogen and hydrogen:



Both these reactions entail an increase in the number of moles of gas (2:3 for the iron nitriding and 1:2 for the ammonia decomposition), which means an overall loss of hydrogen atoms from the system. This will be reflected in a decrease in the background scattering per mole of gas.

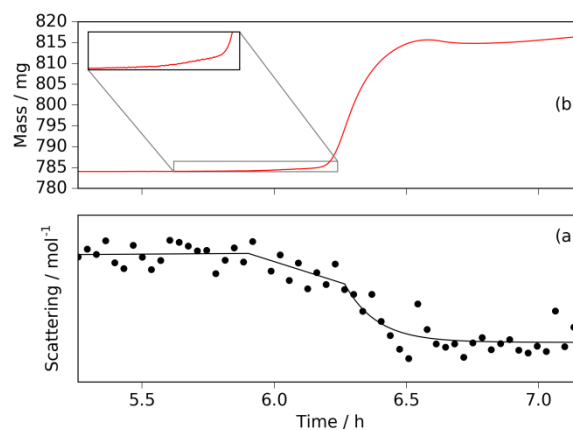


Figure 6: (a) scattering per mole of gas in the IGAⁿ chamber; (b) sample mass.

Such a decrease is visible in the first nitriding period between 5.25 h and 7.2 h (corresponding to region A in Figure 5(b)), where the difference between the initial scattering per gas mole before 5.3

h and the end scattering per gas mole after 7.0 h is marked, Figure 6. Furthermore, this decrease in scattering per mole starts at around 5.9 h, which matches the time when the sample mass starts to increase (see Figure 6(b) inset). As the nitriding reaction rate increases (the temperature was increasing at 4 °C/min at this point), there is a concurrent decrease in the background scattering. This decrease in scattering, however, is almost entirely a consequence of ammonia decomposition (reaction (2)) rather than an increase in gas due to metal nitriding (reaction (1)), since, in the latter case, the relative sizes of the iron sample (784 mg) and the volume of the IGA chamber ($>3 \text{ dm}^3$) means that nitriding can only contribute to a small fraction of the scattering per gas mole decrease; the plateau in Fe_4N formation until the ammonia is refreshed also indicates that the ammonia has decomposed (since there is initially more than enough ammonia to nitride the entirety of the iron sample). This is consistent with the clear decrease (shown as a linear fit) at 5.9 h in scattering compared with the relatively small increase in the sample mass at the same time. From these data, it is possible to conclude, therefore, that ammonia decomposition starts at the same time as the iron nitriding reaction begins. There are two possibilities for this observation: either (i) the ammonia decomposition requires a nitrided iron surface in order to proceed, or (ii) the same rate-limiting step is responsible for both the ammonia decomposition and the formation of iron nitride. It is difficult from these data alone to differentiate the initial cause of ammonia decomposition between the two possibilities of a requiring a nitrided iron surface or N–H bond scission being the coincidental rate-limiting step for ammonia decomposition and iron nitriding. However, given that previous work has found that ammonia decomposes significantly more rapidly (shown by detailed thermogravimetric studies to be by a factor of four) on iron surfaces than on iron nitride surfaces,^{18,19} it is inferred that the rate-limiting step is the same for both nitride formation and ammonia decomposition rather than the latter requiring the former.

A closer inspection of the data when the system was under 2 bar of NH_3 (region B in Figure 5(b)) reveals a similar reduction in the incoherent scattering per gas mole, Figure 7. The rate of reduction is relatively slow initially (for times $< 10.8 \text{ h}$), but there is an increase in that rate at time = 10.8 h, which coincides with when the temperature was increased to 480 °C (from 450 °C). There is very little change in the mass associated with the larger decrease in incoherent scattering per mole apart from the aforementioned loss of the small amount of Fe_3N . The decrease in incoherent scattering per gas mole after time = 10.8 h can be fitted to an exponential decay with a time constant of 0.34(6) h.

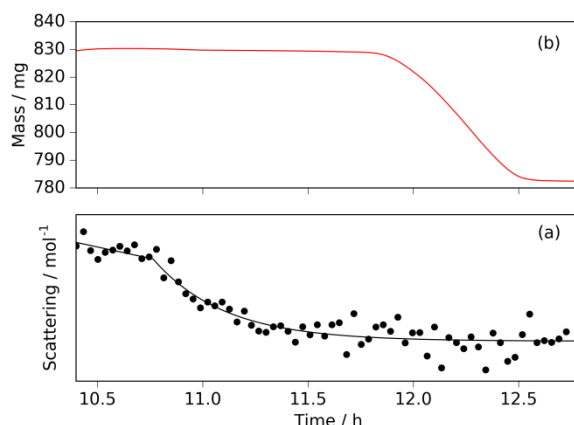
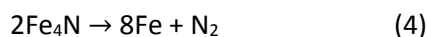


Figure 7: (a) scattering per mole of gas in the IGAⁿ chamber; (b) sample mass.

At 11.8 h, when the incoherent scattering per gas mole has begun to flatten out (i.e. the majority of the ammonia has decomposed), there is a significant decrease in mass of the sample, such that all the Fe₄N has denitrided to become Fe by 12.5 h. (This denitriding reaction is not seen in the scattering per gas mole data, thus confirming that the volumes of gas consumed or released by nitriding or denitriding are too small to significantly affect the overall gas composition.) The metal denitriding reaction may proceed by one of two pathways: either the reverse of reaction (1),



or independently of the hydrogen present in the system,



Both these reactions could be affected by the ammonia decomposition reaction. If reaction (3) is the dominant pathway for denitriding, this is explained by the ammonia decomposing into nitrogen and hydrogen, therefore increasing the hydrogen partial pressure. If reaction (4) is the dominant denitriding pathway, then this is explained by the ammonia partial pressure decreasing and so the rate of nitriding (reaction (1)) decreases, whereas the denitriding reaction rate is unaffected.

Effect of ammonia pressure on the iron denitriding reaction

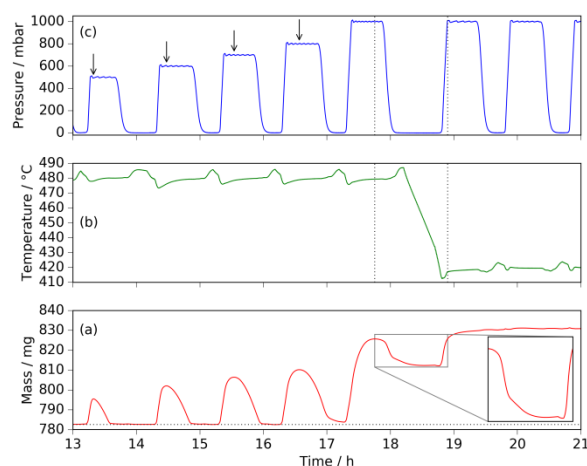


Figure 8: (a) sample mass (with a horizontal dotted line coincident with initial sample mass, left edge of magnified inset region is coincident with sample mass local maximum); (b) sample temperature (with vertical dotted lines aligned with edge of sample mass zoomed inset region); (c) pressure (arrows show pressure at sample mass maxima, vertical dotted lines aligned with edge of sample mass magnified inset region).

Further light can be shed on the nature of the denitrating reaction by inspection of the sample mass under varying ammonia pressures (the part of the experiment for which there exists only partial neutron diffraction data); see Figure 8. For each ammonia pressure region between 500 mbar and 800 mbar (in 100 mbar steps), the sample mass rises ($\text{Fe} \rightarrow \text{Fe}_4\text{N}$), reaches a maximum and falls again ($\text{Fe}_4\text{N} \rightarrow \text{Fe}$). As the pressure of ammonia is increased, the sample mass maxima occur at longer times after ammonia is introduced (shown by the arrows in Figure 8(c)), which directly correlates with the size of the sample mass maxima and the pressure, Figure 9. For all pressures the sample mass begins to fall before the gas is evacuated—i.e. when the gas is a mixture of ammonia, nitrogen and hydrogen. These observations could again be consistent with denitrating proceeding via either reaction (3) or reaction (4) (since both become more favoured as ammonia decomposes).

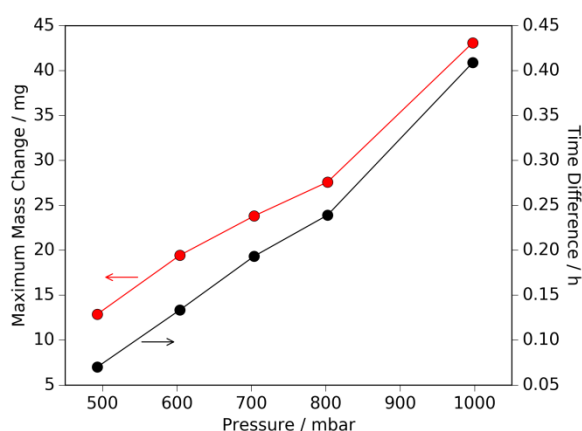


Figure 9: Relationship of the sample mass maxima and the time taken to reach those maxima against the NH_3 pressure introduced (in the region of time = 13–18 h; lines are a guide to the eye).

A closer look at the sample mass rise and fall at 800 mbar (between time = 16–17 h) shows that the sample mass change does not quite reach zero, but does not stop decreasing until more ammonia is introduced (at 1 bar). At 1 bar, this effect is more marked—the sample mass decreases rapidly while there is still gas present, but once the pressure is approximately 0 bar then the sample mass still decreases, but much less rapidly (see inset to Figure 8(a)). When the temperature is lowered from 480 °C to 420 °C, this sample mass decrease stops (at around 450 °C) and the reintroduction of ammonia leads to complete nitriding of the iron sample (which stays as Fe₄N throughout the rest of the experiment). From these observations, it is possible to attribute the rapid decrease in sample mass to denitriding that proceeds through reaction (3) in the presence of hydrogen partial pressure, whereas the slow decrease in sample mass must be denitriding that proceeds via reaction (4) when no hydrogen is present. Therefore, it is clear that denitriding occurs via both routes, but that the mechanism involving hydrogen (to form ammonia, reaction (3)) is more rapid. This is consistent with the known kinetic difficulty **desorbing N₂** (this is the rate-limiting step in ammonia decomposition).

Further information can be elucidated from the shapes of the sample mass traces on denitriding. When denitriding occurs under hydrogen partial pressure, then the mass decrease accelerates until either all Fe₄N is converted to iron or the hydrogen and other gases are evacuated. This indicates that the denitriding via reaction (3) is zeroth order with respect to Fe₄N, i.e. that the movement of nitrogen within the nitride to N_(ads) species on the surface is rapid (not rate-limiting). When there is no hydrogen present and the denitriding proceeds via reaction (4), then the decrease in sample mass is linear (see Figure 8(a)), which again indicates that the denitriding reaction is zeroth order with respect to Fe₄N. This is also consistent with the nitrogen forming N_(ads) species being rapid and the 2N_(ads) → N_{2(g)} being relatively slow. These observations mean that, as discussed above, in the case of ammonia decomposition, nitrogen movement through the lattice is therefore unlikely to be the initial rate-determining step, which leaves N–H scission, which is consistent with previous studies.¹⁶

Implications for the design of ammonia decomposition catalysts

Given that iron surfaces are known to catalyse ammonia decomposition better than iron nitride surfaces,^{18,19,21} then the data presented above yield some considerations about design of ammonia decomposition systems based on iron catalysts. First, lower temperatures favour the nitriding reaction, therefore with higher temperatures a double kinetic benefit is gained in the nature of the catalyst along with the standard increase in reaction rate with increased temperature. Secondly, even small ammonia partial pressures (i.e. in this case, when the ammonia partial pressure is significantly lower than the hydrogen partial pressure) will favour nitride formation over denitriding,

which means that the ammonia decomposition reaction should be run as close to completion as possible in order to avoid nitride formation. Both implications from these considerations (higher temperatures and lower ammonia partial pressures) are desirable for running ammonia decomposition reactions, but the reverse implication is also noteworthy, that performing ammonia decomposition over iron catalysts at low temperatures or with high flows (and thus high ammonia partial pressures) yields the penalty of iron nitride formation. This implication means that iron may not be the ideal catalyst for lower temperature ammonia decomposition.

CONCLUSIONS

The simultaneous use of thermogravimetric analysis and neutron diffraction enables the in-situ analysis of nitride formation and ammonia decomposition over iron catalysts. The iron is found to exist either as iron itself or Fe_4N , with the formation of Fe_3N not being favoured without sufficient ammonia partial pressure. The data suggest that the rate-limiting step for both iron nitriding and initially for ammonia decomposition is N–H scission, whereas the denitriding reaction happens via two possible pathways, either by hydrogen reacting with surface nitrogen to form ammonia or by desorption of nitrogen gas. In this latter case, nitrogen desorption is likely to be the rate-limiting step, which is consistent with the rate-limiting step for ammonia decomposition (once there is some hydrogen gas in the system). Iron is the favoured form of the catalyst at higher temperatures and higher rates of ammonia decomposition, whereas the nitride requires a sufficient ammonia partial pressure to be present.

AUTHOR INFORMATION

Corresponding Authors

thomas.wood@stfc.ac.uk, bill.david@stfc.ac.uk

Funding Sources

This work was financially supported by an EPSRC grant “Fuel Cell Technologies for an Ammonia Economy”, EP/M014371/1. JWM would like to thank St John’s College for financial support.

Notes

The authors declare no competing financial interest

Acknowledgments

The authors acknowledge Paul McIntyre, Adam Sears, James Taylor and Ronald Smith for technical assistance, Charlotte Kirk for help with monitoring the experiment and Alan Soper for provision of neutron scattering data for silica.

REFERENCES

- (1) "Nitrogen (Fixed)—Ammonia", U.S. Geological Survey, Mineral Commodity Summaries, 2017.
- (2) Green L., Jr. "An ammonia energy vector for the hydrogen economy" *Int. J. Hydrogen Energy* **1982**, *7*, 355–359.
- (3) Klerke, A.; Christensen, C. H.; Nørskov, J. K.; Vegge, T. "Ammonia for hydrogen storage: challenges and opportunities" *J. Mater. Chem.* **2008**, *18*, 2304–2310.
- (4) Schüth, F.; Palkovits, R.; Schlögl, R.; Su, D. S. "Ammonia as a possible element in an energy infrastructure: catalysts for ammonia decomposition" *Energy Environ. Sci.* **2012**, *5*, 6278–6289.
- (5) Michikawauchi, R.; Ito, Y. Internal Combustion Engine, U.S. Patent No. 8,240,277, 2012.
- (6) Kordesch, K.; Hacker, V.; Gsellmann, J.; Cifrain, M.; Faleschini, G.; Enzinger, P.; Fankhauser, R.; Ortner, M.; Muhr, M.; Aronsson, R. R. Alkaline fuel cells applications *J. Power Sources* **2000**, *86*, 162–165.
- (7) Ganley, J. C. An intermediate-temperature direct ammonia fuel cell with a molten alkaline hydroxide electrolyte *J. Power Sources* **2008**, *178*, 44–47.
- (8) Grieve, M. J.; Fisher, G. B. Energy conversion device including a solid oxide fuel cell fueled by ammonia, U.S. Patent No. 8,034,499, 2011.
- (9) M. Comotti and S. Frigo, Hydrogen generation system for ammonia–hydrogen fuelled internal combustion engines, *Int. J. Hydrogen Energy*, 2015, **40**, 10673–10686.
- (10) Saadatjou, N.; Jafari, A.; Sahebdehfar, S. Ruthenium Nanocatalysts for Ammonia Synthesis: A Review *Chem. Eng. Commun.* **2015**, *202*, 420–448.
- (11) W. I. F. David, J. W. Makepeace, S. K. Callear, H. M. A. Hunter, J. D. Taylor, T. J. Wood and M. O. Jones, Hydrogen Production from Ammonia using Sodium Amide, *J. Am. Chem. Soc.*, 2014, **136**, 13082–13085.
- (12) J. W. Makepeace, T. J. Wood, H. M. A. Hunter, M. O. Jones and W. I. F. David, Ammonia decomposition catalysis using non-stoichiometric lithium imide, *Chem. Sci.*, 2015, **6**, 3805–3815.
- (13) J. Guo, P. Wang, G. Wu, A. Wu, D. Hu, Z. Xiong, J. Wang, P. Yu, F. Chang, Z. Chen and P. Chen, Lithium Imide Synergy with 3d Transition-Metal Nitrides Leading to Unprecedented Catalytic Activities for Ammonia Decomposition, *Angew. Chem. Int. Ed.*, 2015, **54**, 2950–2954.
- (14) J. Guo, F. Chang, P. Wang, D. Hu, P. Yu, G. Wu, Z. Xiong and P. Chen, Highly Active MnN–Li₂NH Composite Catalyst for Producing CO_x-Free Hydrogen, *ACS Catal.*, 2015, **5**, 2708–2713.
- (15) Ertl, G.; Huber, M. Mechanism and kinetics of ammonia decomposition on iron *J. Catal.* **1980**, *61*, 537–539.
- (16) K. Tamaru, A "new" general mechanism of ammonia synthesis and decomposition on transition metals, *Acc. Chem. Res.*, 1988, **21**, 88–94.
- (17) H. Shindo, C. Egawa, T. Onishi and K. Tamaru, Reaction Mechanism of Ammonia Decomposition on Tungsten, *J. Chem. Soc., Faraday Trans.*, 1980, **76**, 280–290.
- (18) Arabczyk, W.; Zmłyny, J. Study of the ammonia decomposition over iron catalysts *Catal. Lett.* **1999**, *60*, 167–171.
- (19) Arabczyk, W.; Pelka, R. Studies of the Kinetics of Two Parallel Reactions: Ammonia Decomposition and Nitriding of Iron Catalyst *J. Phys. Chem. A* **2009**, *113*, 411–416.
- (20) Feyen, M.; Weidenthaler, C.; Güttel, R.; Schlicke, K.; Holle, U.; Lu, A.-H.; Schüth, F. High-Temperature Stable, Iron-Based Core–Shell Catalysts for Ammonia Decomposition *Chem.–Eur. J.* **2011**, *17*, 598–605.
- (21) Kiełbasa, K.; Pelka, R.; Arabczyk, W. Studies of the Kinetics of Ammonia Decomposition on Promoted Nanocrystalline Iron Using Gas Phases of Different Nitriding Degree *J. Phys. Chem. A* **2010**, *114*, 4531–4534.